Astronomy
&
Astrophysics

O^{18}O and C^{18}O observations of ρ Ophiuchi A*,**

R. Liseau[1], B. Larsson[2], P. Bergman[1], L. Pagani[3], J. H. Black[1], Å. Hjalmarson[1], and K. Justtanont[1]

[1] Department of Radio and Space Science, Chalmers University of Technology, Onsala Space Observatory, 439 92 Onsala, Sweden
    e-mail: firstname.familyname@chalmers.se
[2] Department of Astronomy, Stockholm University, AlbaNova, 106 91 Stockholm, Sweden
    e-mail: bem@astro.su.se
[3] LERMA, L'Observatoire de Paris, 61 avenue de l'Observatoire, 75014 Paris, France
    e-mail: laurent.pagani@obspm.fr

Received 29 October 2009 / Accepted 5 December 2009

ABSTRACT

Context. Contrary to theoretical expectation, surprisingly low concentrations of molecular oxygen, O_2, have been found in the interstellar medium. Telluric absorption makes ground based O_2 observations essentially impossible and observations had to be done from space. Millimetre-wave telescopes on space platforms were necessarily small, which resulted in large, several arcminutes wide, beam patterns. Observations of the ($N_J = 1_1-1_0$) ground state transition of O_2 with the Odin satellite resulted in a $\gtrsim 5\sigma$ detection toward the dense core ρ Oph A. At the frequency of the line, 119 GHz, the Odin telescope has a beam width of $10'$, larger than the size of the dense core.
Aims. The precise nature of the emitting source and its exact location and extent are therefore unknown. The current investigation is intended to remedy this.
Methods. Although the Earth's atmosphere is entirely opaque to low-lying O_2 transitions, it allows ground based observations of the much rarer $^{16}O^{18}O$ in favourable conditions and at much higher angular resolution with larger telescopes. In addition, ρ Oph A exhibits both multiple radial velocity systems and considerable velocity gradients. Extensive mapping of the region in the proxy C^{18}O ($J = 3-2$) line can be expected to help identify the O_2 source on the basis of its line shape and Doppler velocity. Line opacities were determined from observations of optically thin $^{13}C^{18}O$ ($J = 3-2$). During several observing periods, two C^{18}O intensity maxima in ρ Oph A were searched for O^{18}O in the (2_1-0_1) line at 234 GHz with the 12 m APEX telescope. These positions are associated also with peaks in the mm-continuum emission from dust.
Results. Our observations resulted in an upper limit on the integrated O^{18}O intensity of $\int T_A^* d\upsilon < 0.01$ K km s^{-1} (3σ) into the $26\rlap{.}''5$ beam. Together with the C^{18}O data, this leads to a ratio of $N(C^{18}O)/N(O^{18}O) > 16$. Combining Odin's O_2 with the present O^{18}O observations we infer an O_2 abundance $5 \times 10^{-7} < X(O_2) \lesssim 2.5 \times 10^{-6}$.
Conclusions. Examining the evidence, which is based primarily on observations in lines of O^{18}O and C^{18}O, leads us to conclude that the source of observed O_2 emission is most likely confined to the central regions of the ρ Oph A core. In this limited area, implied O_2 abundances could thus be higher than inferred on the basis of Odin observations (5×10^{-8}) by up to two orders of magnitude.

Key words. ISM: abundances – ISM: molecules – ISM: lines and bands – ISM: clouds – ISM: individual objects: ρ Oph A SM 1 – ISM: individual objects: ρ Oph A SM 1N

1. Introduction

Oxygen is the most abundant of the astronomical metals (e.g., Asplund et al. 2009, and references therein). Consequently, in its molecular form, it was also expected to be very abundant in the UV-shielded regions inside molecular clouds (e.g., Black & Smith 1984; Bergin et al. 2000; Charnley et al. 2001; Roberts & Herbst 2002; Spaans & van Dishoeck 2001; Viti et al. 2001; Willacy et al. 2002; Quan et al. 2008) and to contribute significantly to the cooling, hence the energy balance, of dense clouds (Goldsmith & Langer 1978).

Because of the high O_2 content in the Earth's atmosphere, astronomical O_2 sources cannot be observed from the ground.

Dedicated space missions[1] came into operation near the beginning of the new millenium. Their unsuccessful searches (Goldsmith et al. 2000; Pagani et al. 2003) were highly disappointing and it was hard to understand that, in the interstellar medium (ISM), O_2 is an elusive species (see references cited above).

Eventually, after more than 20 days of Odin-observing during three different runs, came a real break-through: for the very first time, O_2 was finally detected in the ISM (Larsson et al. 2007). The O_2 emitting object, ρ Oph A, is a dense clump (Loren et al. 1990) in a region of active star formation (L 1688). On the basis of theoretical model calculations, the detectability of this kind of source had earlier been predicted by Black & Smith (1984) and Maréchal et al. (1997a), where the latter authors made their specific prediction with regard to Odin.

Odin carries a 1.1 m telescope which is designed for observations in the submillimetre regime, between roughly 480 and

---

* Based on observations with APEX, Llano Chajnantor, Chile.
** Data cubes of Figs. 3 and 4 are only available in electronic from at the CDS via anonymous ftp to
cdsarc.u-strasbg.fr (130.79.128.5) or via
http://cdsweb.u-strasbg.fr/cgi-bin/qcat?J/A+A/510/A98

[1] SWAS in 1998, see http://cfa-www.harvard.edu/swas/, and Odin in 2001, see http://www.snsb.se/eng_odin_intro.shtml

580 GHz (0.5–0.6 mm). However, the O_2 discovery was made with a dedicated 119 GHz (2.5 mm) receiver aboard Odin, fixtuned to the frequency of the ground state O_2 ($N_J = 1_1-1_0$) transition at 118 750.343 MHz. At this frequency, the telescope beam size is $10'$, larger than the angular dimension of the dense ρ Oph A core, which is about $4'$ (*FWHM* of devonvolved CS core, Liseau et al. 1995).

It follows that the true O_2 source is likely under-resolved, the consequence of which directly affects estimates of the abundance of O_2, i.e. $N(O_2)/N(H_2)$: depending on the adopted model, the Odin observations imply an abundance which is currently uncertain by two orders of magnitude (Liseau et al. 2005).

In Fig. 2 of Larsson et al. (2007), the Odin-O_2 line is compared to transitions of other molecular species in ρ Oph A. Whereas lines of H_2O and CO are optically very thick over large parts of the cloud and have self-absorbed profiles, the optically thin O_2 line displays a simple, Gaussian shape. This line shape is similar to that of the C $158\,\alpha$ line (Pankonin & Walmsley 1978), displayed at the top of the figure and which most likely originates in the ρ Oph-PDR. If also the main source of O_2 emission, the abundance would indeed be very low.

However, the O_2 line shape is also similar to that of the $C^{18}O$ (3−2) line, also shown in the figure. This suggests that the $C^{18}O$ line can be used as a tracer of the molecular oxygen emission and we set out to map the $10'$ Odin beam in the (3−2) transition of $C^{18}O$ with the APEX beam of size $19''$. It was expected that a detailed comparison of the line centre velocity with that of the O_2 line would help to narrow down the exact location of the O_2 emission, since two distinct velocity components are known to be present in ρ Oph A. This information is needed to understand, where, i.e. in what physical conditions, the majority of the O_2 molecules is excited: in the cold and dense dark cores (Di Francesco et al. 2004), in the extended warm Photon Dominated Region (PDR; Hollenbach et al. 2009) or in the hot shocked gas of the outflow from VLA 1623 (Liseau & Justtanont 2009)? With the $C^{18}O$ proxy for O_2 emission, probable emission regions were identified, which were then observed for $^{16}O^{18}O$ (2_1-0_1).

There exists earlier work for this line and the ρ Oph cloud. Goldsmith et al. (1985) observed ρ Oph A in the same transition and with comparable beam size ($26''$), albeit at an offset $11''$ E and $61''$ N relative to the position of SM 1N. They obtained $T_R^* < 120$ mK (1σ) over 0.34 km s^{-1}. At similar channel resolution (0.32 km s^{-1}) and toward essentially the same position, Liszt & Vanden Bout (1985) obtained an rms-noise value of $T_R^* < 17.5$ mK with the 12 m NRAO telescope ($34''$). These papers also present energy level diagrams. Observations made with the 10 m telescope of the Caltech Submillimeter Observatory (CSO) in July 1991 and for the position $16^h23^m25^s$, $-24°15'49''$ (B1950)[2] resulted in an rms noise temperature of 16 mK in a 0.25 km s^{-1} velocity bin and of 12 mK after binning to 0.50 km s^{-1} (van Dishoeck, Keene, & Phillips, private communication).

The derivation of molecular abundances requires knowledge of the H_2 column density. One of the widely exploited techniques to estimate $N(H_2)$ is to use observations of $C^{18}O$, the transitions of which in many cases can be shown to be optically thin. We discovered, however, that in the dense core regions of ρ Oph A, this not to be the case everywhere and that appropriate opacity corrections using the $^{13}C^{18}O$ line needed to be made.

This paper is organised as follows: in Sect. 2, our APEX observations of the ρ Oph A cloud in transitions of $O^{18}O$, $C^{18}O$ and $^{13}C^{18}O$ are described. Section 3 presents our results, which are discussed in Sect. 4. Finally, in Sect. 5 our main conclusions are briefly summarised.

2. Observations and data reductions

All observations have been made with the SIS receivers and spectrometers at the Atacama Pathfinder EXperiment (APEX). The 12 m APEX telescope is located at an altitude of about 5100 m on the Llano de Chajnantor in northern Chile[3]. The telescope pointing is accurate to $3''$ (rms).

The Fast Fourier Transform Spectrometer (FFTS) was configured to have 8192 channels, which over a bandwidth of 1 GHz provides a resolution of 122 kHz, corresponding to 0.16 km s^{-1} and 0.11 km s^{-1} at 234 GHz and 329 GHz, respectively. As frontends for these frequencies, we used APEX 1 of the Swedish Heterodyne Facility Instrument (SHFI, Vassilev et al. 2008) and APEX 2A (Risacher et al. 2006).

2.1. $O^{18}O$ observations

The data have been collected during three different observing runs in 2008 and 2009. The frequency of the (2_1-0_1) line can be derived from the data given by Steinbach & Gordy (1975) as 23 3946.179 MHz. At 234 GHz, the APEX beam has a half power beam width HPBW = $26''5$ and the main beam efficiency is $\eta_{mb} = 0.75$. The telescope was pointed toward RA = $16^h26^m27^s2$ and Dec = $-24°23'34''$ (J2000), a position which was initially chosen on the basis of, as it turned out, insufficiently sampled data (see Sect. 3.2). In addition, the strongest peak of doubly deuterated formaldhyde emission in the ρ Oph A core (Bergman et al., in preparation)[4], which is situated $30''$ south of these coordinates, was also observed. These positions are close to the location of intense mm-dust-emission (cf. Fig. 3), i.e. the dense core SM 1 (Motte et al. 1998). For the primary position, the total on-source integration time was 4.9 h and the average system temperature was $T_{sys} \sim 220$ K, whereas for the $-30''$-position, these values were 6.5 h and 210 K, respectively.

2.2. $C^{18}O$ and $^{13}C^{18}O$ observations

The observations were collected during two observing runs in 2006 and 2007 at the APEX telescope. The observing mode was position switched raster mapping and the data were sampled according to the Nyquist criterion on a rectangular $10''$ grid, aligned with the equatorial coordinate system ($200'' \times 200''$). At 329 GHz, the HPBW = $19''$ and the average system temperature was $T_{sys} = 200$ K. The efficiencies were $\eta_{mb} = 0.73$ and $\eta_{Moon} = 0.85$ for point source and extended source calibrations, respectively.

In addition, an extended raster map of the outer regions of ρ Oph A was obtained on a coarser grid with $20''$ (full beam) spacings. The entire region observed is thus as large as $\Delta\alpha \times \Delta\delta = 10' \times 5'$.

The origin of the map is the same as that of the Odin observations, i.e. the (0, 0) position is at RA = $16^h26^m24^s6$ and Dec = $-24°23'54''$ (J2000). The same reference position as for the Odin observations (Larsson et al. 2007), viz. $15'$ N relative

---

[2] This corresponds to $16^h26^m26^s4$, $-24°22'33''$ in J2000 coordinates and is at ($+25''$, $+80''$) relative to the origin of the $C^{18}O$ map (Fig. 3).

[3] http://www.apex-telescope.org/

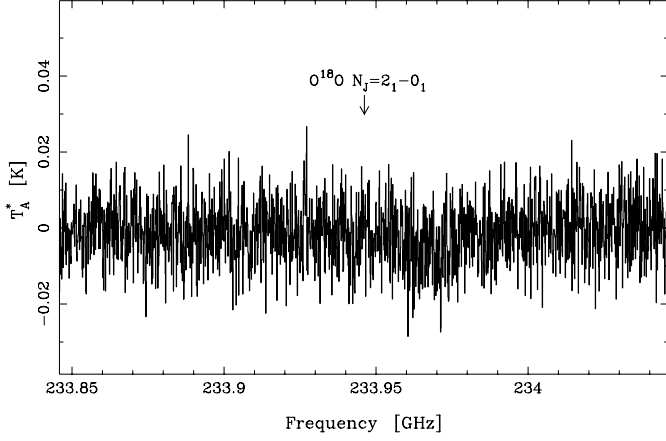[4] The 234 GHz spectra admitted also lines of deuterated formaldehyde. Mapping observations revealed this peak position.

Fig. 1. The central part of the 1 GHz wide APEX spectrum centered on the frequency of the ^{16}O^{18}O (2_1-0_1) transition, 233.946179 GHz, and obtained toward RA = 16^{h}26^{m}27.2 and Dec = $-24°24'04''$ (J2000) in ρ Oph A. The sampling is in 122 kHz wide channels ($\delta\upsilon = 0.16$ km s^{-1}).

Table 1. C^{18}O-peaks of integrated intensity, $\int T_A^* d\upsilon$.

C^{18}O-peak	Offset (arcsec)	RA (J2000)	Dec (J2000)	Other ID
P 1	+35, +50	16:26:27.2	-24:23:04	N 1
P 2	+45, +28	16:26:27.9	-24:23:26	N 5, SM 1N
P 3	+45, -13	16:26:27.9	-24:24:07	N 4, SM 1
P 4	+48, +75	16:26:28.1	-24:22:39	16264-2422b

Notes. *N*-sources from Di Francesco et al. (2004), SM-objects from Motte et al. (1998), RA-Dec labelled source from Johnstone et al. (2000).

to the map centre, was used here for calibration purposes. In addition to the C^{18}O map, five positions were also observed in the $(3-2)$ transition of the even rarer isotope ^{13}C^{18}O (Table 2). Klapper et al. (2003) provide lab-frequencies for the $(3-2)$ rotational transition of C^{18}O and ^{13}C^{18}O, i.e., 329 330.552 MHz and 314 119.660 MHz, respectively, and where the latter is a weighted mean value, with the ^{13}C hyperfine structure being ignored.

3. Results

3.1. O^{18}O

The ^{16}O^{18}O (2_1-0_1) line was not detected toward any of the observed positions. Toward the position associated with P 2 (see Fig. 3 and Table 1), the noise level is $T_{rms} = 6.5$ mK (1σ) in a 0.62 km s^{-1} bin. The result is similar for the observation of the position 30$''$ south (P 3), i.e., $T_{rms} = 8.2$ mK in a 0.16 km s^{-1} bin (Fig. 1).

3.2. C^{18}O and ^{13}C^{18}O

Example spectra in three isotopes of CO $(3-2)$ are shown in Fig. 2 toward two positions in the central region of the ρ Oph A core. Further, Fig. 3 shows the inner, high-resolution, map of integrated intensity, $\int T_A^* d\upsilon$, of the C^{18}O $(3-2)$ line. Within a range of RA offsets +30$''$ to +50$''$, four distinct intensity peaks are discernable. In Table 1, these are designated P 1 through P 4 and their J2000 coordinates are given. The C^{18}O line is very narrow, e.g. merely 1.0 km s^{-1} (*FWHM*) at the inconspicuous (0, 0) position.
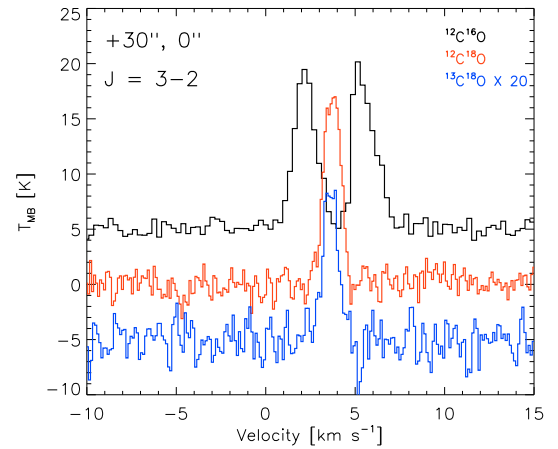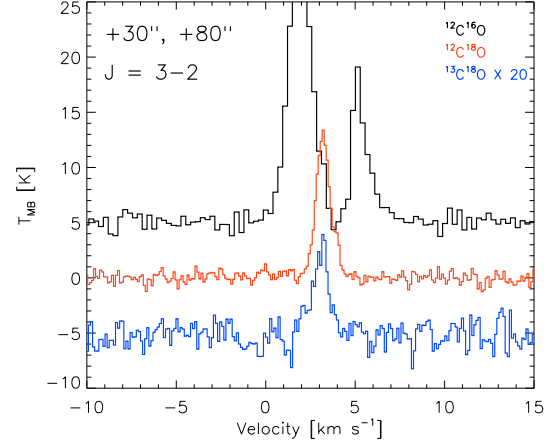

Fig. 2. $(J = 3-2)$ spectra (T_{mb} vs. υ_{LSR}) of, *from top to bottom*, CO (black), C^{18}O (red) and ^{13}C^{18}O (blue) toward two positions in the ρ Oph A core (cf. Fig. 3). For clarity, two of the spectra are offset by ± 5 K and the ^{13}C^{18}O spectra have been multiplied by a factor of twenty.
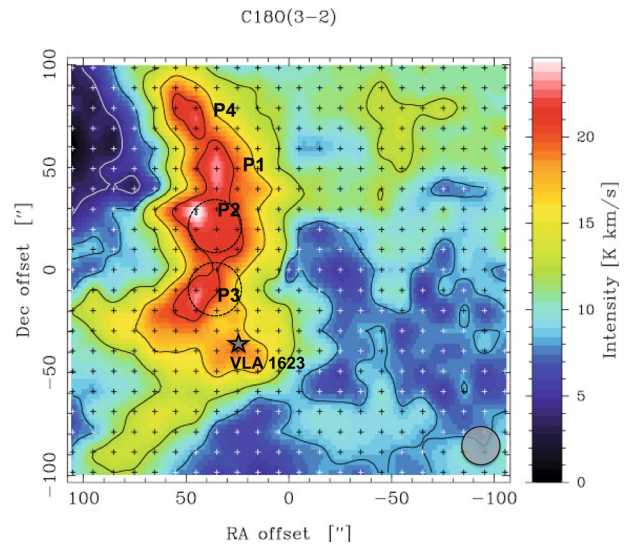

Fig. 3. C^{18}O $(3-2)$ integrated intensity, $\int T_A^* d\upsilon$, of the dark core ρ Oph A. The map was obtained with APEX and observed positions are shown as crosses. The beam size at 329 GHz is shown in the lower right corner. Offsets are with respect to the origin, RA = 16^{h}26^{m}24.6 and Dec = $-24°23'54''$ (J2000). The position of the outflow driving Class 0 source VLA 1623 is shown by the star symbol. P 1-P 4 designate the clumps discussed in the text (Table 1). The beam size at 234 GHz is indicated by the dotted circles, at the observed O^{18}O positions.
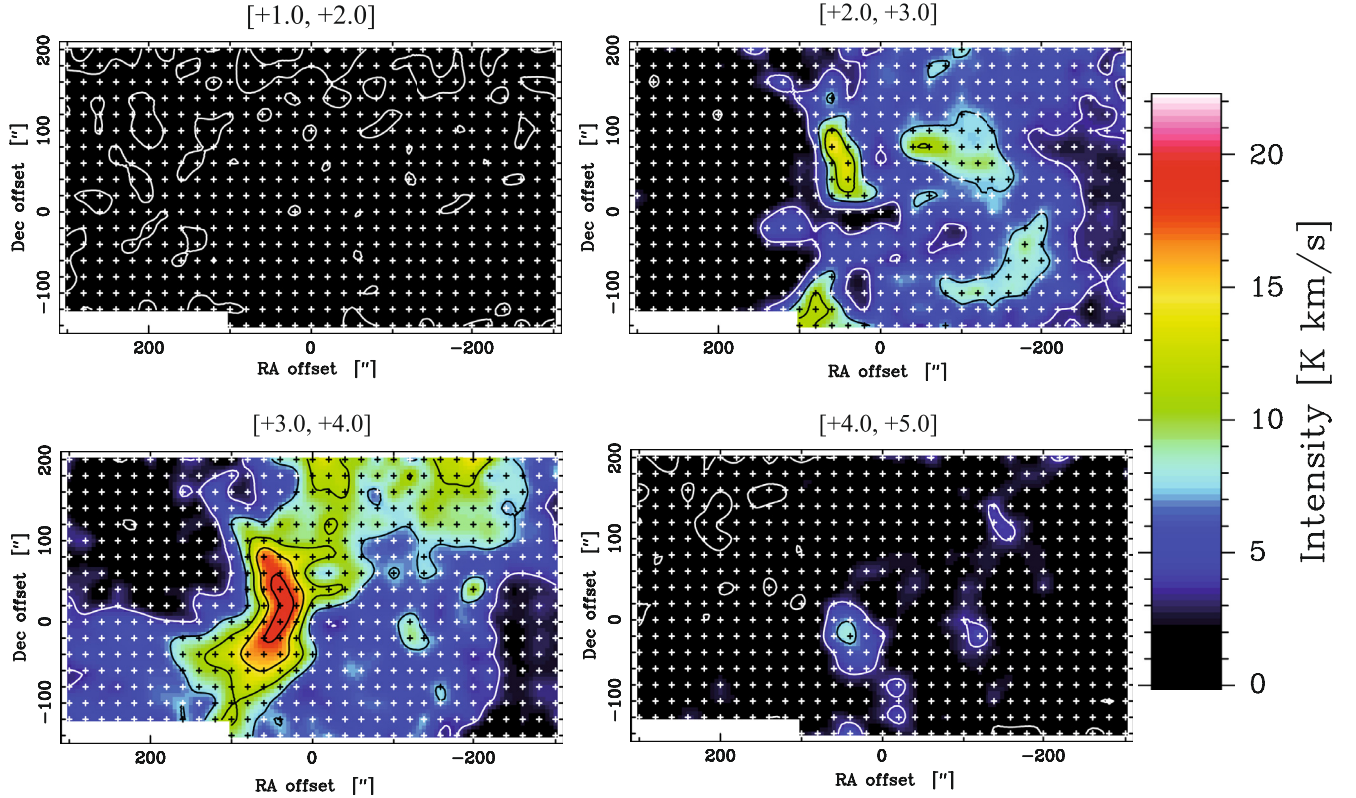
Fig. 4. A mosaic of maps of integrated $C^{18}O$ (3−2) line intensity over 1.0 km s^{-1} wide velocity intervals, from +1.0 to +5.0 km s^{-1}. The extended maps with 20″ spacing are shown. Two velocity components are identified in the ρ Oph A core, falling into the [2, 3] and [3, 4] bins, respectively. The lowest contour level corresponds to 4 K km s^{-1} and increments are also by this amount.

Examination of the entire data set for $C^{18}O$ (3−2) reveals the fact that, within the mapped region, maximum emission occurs at LSR-velocities +2.7 to +3.7 km s^{-1}. This velocity interval corresponds to that of the O_2 119 GHz emission, viz. $v_{LSR} \sim +2.5$ to +3.5 km s^{-1} (Larsson et al. 2007) and Fig. 6 here. ρ Oph A displays a complex velocity field and two distinct velocity components can be identified, giving rise to spectral line blending. These components are essentially confined within the LSR-velocity bins [+2, +3] and [+3, +4] (in km s^{-1}). Figure 4 presents a mosaic of the integrated line intensity in 1.0 km s^{-1} wide bins. Experimenting also with different binnings demonstrates quite convincingly that the location of the O_2 emitting gas is most likely associated with the central core region of ρ Oph A.

4. Discussion

4.1. The dense clumps of ρ Oph A

The $C^{18}O$ intensity maxima in Fig. 3 seem comparable in size with the APEX beam, which could indicate that the diameter of these clumps does not exceed 20″. From the comparison of their locations with those observed in the emission of the dust at 1.3 mm (Motte et al. 1998) and 850 μm (Johnstone et al. 2000) and of the quiescent gas in the N_2H^+ (1−0) line (Di Francesco et al. 2004), it becomes evident that P 4 lacks correspondence with features at 1.3 mm and N_2H^+ emission, but shows up weakly at 850 μm. P 1 likely is N1 (which is not seen in the dust maps), P 2 corresponds to N 5 (also prominent in the dust as SM 1N), and P 3 seems associated with N 4 and SM 1 (also 16264-2423 of Johnstone et al. 2000). Derived temperatures and densities for these clumps are of the order of 15−30 K

and 0.2−5×10^6 cm^{-3}, respectively (e.g., André et al. 1993; Motte et al. 1998; Johnstone et al. 2000).

In summary, the evidence points toward the fact that also O_2 is concentrated in the dense dark core regions, where the molecules would be protected against photo-dissociation due to the intense UV field (G_0 of the order of 10^2) generated by the two B-stars, east and west of the cores, respectively (Liseau et al. 1999). The size of the O_2 emitting regions appears not to exceed one arcminute, so that a conservative estimate of the Odin beam filling would be about 0.01. If the emission originates in a core of size ∼ 20″ or smaller, the Odin beam filling factor would be reduced by yet another order of magnitude. The O_2 abundance would scale accordingly and could in this case be locally as high as a few times 10^{-5}, which would be comparable to the total abundance of oxygen in the gaseous phase (e.g., Liseau & Justtanont 2009).

4.1.1. Line optical depths

The ratio of the $^{13}C^{18}O$ and $^{12}C^{18}O$ line intensities can be used to estimate the optical depth in the rarer isotope line, $\tau_{^{13}C^{18}O} \sim \ln(1 - r_{13})^{-1}$, where $r_{13} \equiv T(^{13}C^{18}O)/T(^{12}C^{18}O)$. From the data presented in Table 2, it is clear that the $C^{18}O$ (3−2) line could have significant opacity along several lines of sight, unless the relative abundance $[^{12}C^{18}O/^{13}C^{18}O] \ll 50$ (or the excitation temperatures for these species differ substantially).

Federman et al. (2003) determined a column density ratio $N(^{12}CO)/N(^{13}CO) = 125 \pm 23$ toward a line of sight designated ρ Oph A by them[5]. However, their coordinates refer to

---

[5] In addition, for their ρ Oph A line of sight, Federman et al. (2003) also give $N(^{12}C^{16}O)/N(^{12}C^{18}O) = 1100 \pm 600$.

Table 2. Observed positions of ^{13}C^{18}O (3–2) and line opacities, $\tau_{^{13}C^{18}O}$.

Offset (arcsec)	υ_{LSR} (km s^{-1})	FWHM (km s^{-1})	$T_{peak}(^{12}C^{18}O)$, $T_{peak}(^{13}C^{18}O)$ (K)	$\tau_{^{13}C^{18}O}$	Note
−60, +80	2.86 ± 0.05	0.78 ± 0.12	10.5, 0.25	0.02	. . .
0, +60	3.13 ± 0.06	0.92 ± 0.14	8.1, 0.22	0.03	. . .
+30, +80	3.09 ± 0.05	1.11 ± 0.09	13.0, 0.38	0.03	P 1
+30, 0	3.62 ± 0.02	1.02 ± 0.05	16.5, 0.71	0.04	P 3
+60, −100	2.95 ± 0.06	1.17 ± 0.15	6.1, 0.23	0.04	2 lines?

Notes. Error on line ratios is estimated at 15–20%.

Table 3. Column densities of C^{18}O and O^{18}O.

T_k (K)	$A_{3,2}/\gamma_{3,2}$ (cm^{-3})	N(C^{18}O) (cm^{-2})	$A_{21,01}/\gamma_{21,01}$ (cm^{-3})^a	N(O^{18}O) (cm^{-2})^b	$\dfrac{N(C^{18}O)}{N(O^{18}O)}$
300	3.4×10^4	4.9×10^{16}	2.7×10^2	$<5.6 \times 10^{15}$	>9
100	4.0×10^4	2.0×10^{16}	4.7×10^2	$<2.0 \times 10^{15}$	>10
40	1.7×10^5	1.2×10^{16}	7.4×10^2	$<9.5 \times 10^{14}$	>14
20	1.7×10^5	1.4×10^{16}	1.0×10^3	$<6.3 \times 10^{14}$	>22
10	1.7×10^5	3.2×10^{16}	1.5×10^3	$<5.5 \times 10^{14}$	>59

Notes. $^{(a)}$ Collision rate coefficient $\gamma(T)$ = 4.9 × 10^{-11} $(T/300\,\mathrm{K})^{0.5}$ cm^3 s^{-1}. $^{(b)}$ Limits on N(O^{18}O) are 1σ; $f_b = 1.0$ and $\int T_A^* d\upsilon < 3.3$ mK km s^{-1}.

the star, one degree north-north-west from the ρ Oph A core discussed in our paper. In the associated nebula, the physical conditions are different from those in the dense core, possibly leading to different isotopic abundances. In the shielded regions of the dense cores, chemical isotopic fractionation can be expected to be of minor importance. It is worth noting that in the nearby ρ Oph core C, a lower isotopic ratio [^{12}C]/[^{13}C] = 65 ± 10 has been derived by Bensch et al. (2001).

4.2. Column densities

If local thermal equilibrium (LTE) is a good approximation for the level populations, the column density of all molecules of the species, N(mol) in cm^{-2}, can be estimated from the observed intensity of an optically thin line, viz.

$$N(\mathrm{mol}) = \frac{\int T_A^* d\upsilon}{f_b\,\eta_{mb}} \times \Phi(T_k) \quad (1)$$

where

$$\Phi(T_k) \equiv \left(\frac{2\,\pi^{1/3}k}{hc}\right)^3 \frac{T_{tr}^2}{A_{ul}} \frac{F(T_k)}{F(T_k) - F(T_{bg})} \frac{Q(T_k)}{g_u} \exp(T_u/T_k) \quad (2)$$

with cgs-units of K^{-1} cm^{-3} s. Here, f_b is the beam filling factor for the source which may be smaller than the beam ($0 \leq f_b \leq 1$) and η_{mb} is the main beam efficiency. $T_{tr} = h\nu/k$ is the transition temperature, $T_{bg} = 2.725$ K is the temperature of the background radiation field, $F(T) \equiv T_{tr}/[\exp(T_{tr}/T) - 1]$ is the quasi-Planck function, T_u is the upper level energy in K, $Q(T_k)$ is the partition function and $g_u = (2J + 1)$ is the statistical weight of the upper level and the other symbols have their usual meaning.

4.2.1. C^{18}O and H$_2$ column densities

We limit the discussion to the central core region, where observed C^{18}O (3–2) line intensities of the +3 km s^{-1} component are $\int T_A^* d\upsilon = 20$ K km s^{-1}. The upper level energy lies nearly 32 K above ground. The spontaneous transition probability for the transition is $A_{32} = 2.158 \times 10^{-6}$ s^{-1}, the transition temperature is $T_{tr} = 15.813$ K and the statistical weight of the upper level is $g_u = 7$. Using the collisional rate coefficients of Schinke et al. (1985) for collisions with para-H$_2$, yields critical densities, $n_{crit} \sim A_{32}/\gamma_{32}(T_k)$, of about 2×10^5 to 3×10^4 cm^{-3} for $T_k = 10$ K to 300 K, respectively (Table 3). Therefore, except perhaps for the very lowest temperatures, the condition of LTE should be fulfilled for the C^{18}O (3–2) transition (cf. Sect. 4.1).

The sizes of the clumps are comparable to the beam size, so that the main beam efficiency, $\eta_{mb} = 0.73$, is used for the intensity calibration and we assume here a beam filling factor of unity. For the broad range of temperatures of 10 to 300 K, the corresponding column densities of C^{18}O are listed in Table 3. For an X(C^{18}O)= 1 to 2×10^{-7}, the derived H$_2$ column densities, on the 20″ scale (2400 AU), are N(H$_2$) = $(1\pm^3_{0.5}) \times 10^{23}$ cm^{-2}. These results are in general agreement with those reported by others (Loren et al. 1990; Motte et al. 1998). Possible opacity corrections to the C^{18}O (3–2) intensity, of the order of $\tau/(1 - \exp -\tau) \gtrsim 2$, would increase the column density accordingly. The column densities presented in Table 3 are therefore likely lower limits.

4.2.2. O^{18}O column density and O^{18}O abundance

The $N_J = 2_1 - 0_1$ transition has the largest Einstein coefficient of the low-lying O^{18}O transitions, viz. $A_{21,01} = 1.33 \times 10^{-8}$ s^{-1} (Maréchal et al. 1997b). We adopt the coefficients for collisional de-excitation, $\gamma_{21,01}(T_k)$, which are based on the work by Bergman (1995) and which have been derived for collisions with He. For collisions with H$_2$, these were multiplied by 1.4. Values for temperatures other than 300 K were obtained by scaling with the square root of the temperature. From Table 3, it can be seen that critical densities for the $2_1 - 0_1$ transition are rather low for a wide range of temperatures (<1500 cm^{-3} above 10 K). In particular, for the dense core conditions of ρ Oph A, where densities are in excess of 10^5 cm^{-3} (Sect. 4.1), LTE is certainly a valid assumption (see also Black & Smith 1984; Maréchal et al. 1997b). The temperature of the transition is $T_u = T_{tr} = 11.228$ K and the statistical weight of the upper level is $g_u = 3$.

In Table 3, the results for C^{18}O and O^{18}O are compared. The ratio N(C^{18}O)/N(O^{18}O) exceeds unity and increases with decreasing temperature. This ratio could correspond to about half the value of that of the CO/O$_2$ ratio (Black & Smith 1984). For three cold cores (10 and 15 K), Fuente et al. (1993) determined CO/O$_2$ > 3–7, limits consistent with, but considerably smaller, than the values displayed in Table 3. The effects of a varying C/O ratio in the ISM at column densities (values of the visual extinction A_V) as high as those found in ρ Oph A were explicitly considered in the models by Maréchal et al. (1997a, see their Fig. 10). For the O$_2$ 119 GHz line, the integrated intensity is >10 K km s^{-1} for C/O < 0.4 when A_V > 20 mag. In contrast, for similar extinction, the intensity is <100 mK km s^{-1} for C/O > 1. Future observations will likely be able to follow any variation
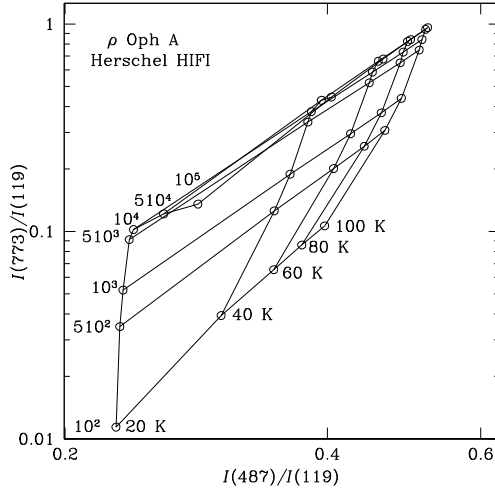
Fig. 5. O_2 line ratio diagram for the two strongest transitions accessible to HIFI aboard the Herschel Space Observatory. In these multitransition calculations, radiation from dust was included and LTE was not assumed. Intensity ratios are relative to the (1_1-1_0) 119 GHz line, which was detected by Odin (24 ± 4 mK km s^{-1} in a 10' beam; Larsson et al. 2007). These transitions are the (3_3-1_2) 487 GHz line (44'') and the (5_4-3_4) 773 GHz line (28''), respectively. Labels along the graph refer to the density, $n(H_2)$ in cm^{-3}, and the gas temperature, T_k in K.
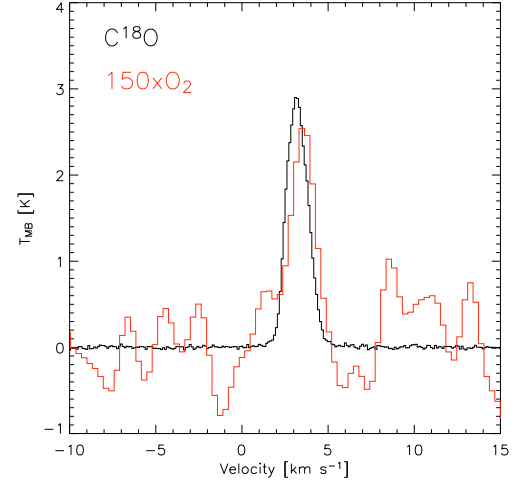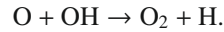

Fig. 6. The line profile of the C^{18}O $(3-2)$ map, after convolution with a 600'' beam, is shown in black and is compared to the scaled O_2 line of Larsson et al. (2007) shown in red. The higher S/N APEX data are spectrally sampled at a higher rate and have also higher resolution. The C^{18}O line intensity is dominated by an extended cloud component at an LSR-velocity seemingly different from that of the P 3 core and the O_2 emission (see also Table 4).

of this ratio in different regions of the ISM (see below and also Black & Smith 1984).

In the dense cold ($\ll 100$ K) regions of the ρ Oph A core, the column density of O^{18}O is lower than 10^{15} cm^{-2} (Table 3) and, hence, the abundance relative to H$_2$, X(O^{18}O) $< 10^{-8}$. Consequently, for the range of 10 to 40 K and a standard elemental isotopic ratio, the abundance of the primary species of molecular oxygen, X(O$_2$) $\sim 500/2 \times X$(O^{18}O) (Wannier 1980), should be limited to $<5 \times 10^{-7}-2 \times 10^{-6}$, consistent with the Odin result (Larsson et al. 2007). We can conclude, therefore, that in the ρ Oph A core, the molecular oxygen abundance is bounded by $5 \times 10^{-8} \leq X$(O$_2$) $< 2.5 \times 10^{-6}$, where the beam averaged O_2 column density is 10^{15} cm^{-2}. If reflecting the fraction of the Odin beam[6] that is filled by the O_2 source, its implied size is $\lesssim 600''/\sqrt{250} = 38''$. This could be well-matched to the 3.5 m telescope of the Herschel Space Observatory[7], the beam widths of which are 44'' at 487 GHz, the frequency of the O_2 ($N_J = 3_2-1_2$) transition, and 28'' at 773 GHz for the $(5_4 - 3_4)$ line (Fig. 5).

4.3. Nature, location and extent of the O_2 source

4.3.1. Oxygen in the cold ISM

The capital letter designation of the cores was introduced by Loren et al. (1990) for the location of emission peaks in lines of DCO$^+$ in the ρ Oph cloud. Depending on the details of the considered models of the deuteration process, they derived kinetic gas temperatures inside the cores which were always low, in the range 18–23 K, whereas temperatures in the outer layers were considerably higher.

---

[6] Odin observations resulted in a column density of oxygen N(O$_2$) = 1×10^{15} cm^{-2} (Larsson et al. 2007). If Ω(O$_2$) = Ω(C^{18}O), the beam filling of the O_2 source is 10^{-3} to 10^{-2}, i.e. the beam corrected N(O$_2$) = $10^{17}-10^{18}$ cm^{-2}. If N(O^{18}O)/N(O$_2$) = 1/250, then the expected column density of isotopic oxygen is likely within 0.4×10^{15} cm$^{-2} \lesssim N$(O^{18}O) $\lesssim 4 \times 10^{15}$ cm^{-2} for a source of size about 20'' to 60''.
[7] http://herschel.esac.esa.int/

In the interstellar medium, it is expected that most of the molecular oxygen is formed by the reaction

$$O + OH \rightarrow O_2 + H.$$

The thermal rate coefficient of this reaction has recently been measured in the laboratory down to temperatures of 39 K (Carty et al. 2006), where it remains rapid. In subsequent ab initio theoretical calculations, Xu et al. (2007) found a much smaller rate at temperatures below 30 K and suggested that this might solve the problem of missing O_2 in cold interstellar clouds. The low-temperature behaviour of the reaction is also of interest for ultra-cold collisions. Quéméner et al. (2009) have determined that the reaction still proceeds in the limit of zero temperature with a rate coefficient of approximately 6×10^{-12} cm^3 s^{-1}. Quan et al. (2008) re-examined the sensitivity of the interstellar O_2 abundance to the low-temperature behaviour of the source reaction.

Also a widely favoured explanation for the generally observed paucity of molecular oxygen in the gas phase is depletion of atomic oxygen with subsequent hydrogenation on cold grain surfaces. This scenario seems supported by several observed molecules. For instance, the hydrogenation of CO is predicted to lead to H$_2$CO, CH$_3$OH and subsequently also the deuterated forms of these species (Matar et al. 2008; Fuchs et al. 2009). In order to become observable, these species have to be returned into the gas phase. Indeed, enhanced emission in methanol and doubly deuterated formaldehyde has been observed toward the centre of ρ Oph A by, respectively, Liseau et al. (2003) and Bergman et al. (in preparation). In addition, widespread emission of gas phase H$_2$O in ρ Oph A is also observed (Larsson et al., in preparation), a fraction of which may have been similarly produced by the hydrogenation of O_2 on cold grain surfaces (Ioppolo et al. 2008). The equilibrium between adsorption and desorption of molecules would then naturally lead to low levels of both species (as compared and in contrast to pure gas phase chemistry).

Table 4. Gaussian parameters of ^{13}C^{18}O (3−2) and O$_2$ (1$_1$−1$_0$) lines.

Molecular spectral line	υ_{LSR} (km s^{-1})	$FWHM$ (km s^{-1})	T_{peak} (K)	Note
O$_2$ 119 GHz	3.5	1.5^a	17.4 × 10^{-3}	observed 10′ beam
C^{18}O 329 GHz	3.2	1.4	2.9	convolved 10′ beam
C^{18}O 329 GHz	3.6	1.0	16.5	observed 19″ beam, P 3

Notes. $^{(a)}$ The O$_2$ line is artifically broadened (see Larsson et al. 2007).

4.3.2. Site and size of the O$_2$ source

Figure 6 shows the C^{18}O (3−2) spectrum after the convolution of the observed map with a 10′ beam. A Gaussian profile provides a good fit to the observed line, the parameters of which are $T_A^* = 2.9$ K, $\upsilon_{LSR} = 3.20$ km s^{-1} and $\Delta\upsilon_{FWHM} = 1.45$ km s^{-1} (Table 4). This velocity is offset from that of the core P 3 (3.62 km s^{-1}, cf. also Table 2) and the intensity is dominated by an extended component. The integrated value is $\int T_A^* d\upsilon = 4.5$ K km s^{-1}. Using the temperature assumed by Larsson et al. (2007, i.e. 30 K) we obtain the beam averaged column density[8] N(C^{18}O) $\geq 2.5 \times 10^{15}$ cm^{-2}. The comparison with the Odin result, i.e. N(O$_2$) $= 1 \times 10^{15}$ cm^{-2}, would indicate that N(C^{18}O)/N(O$_2$) > 1. A C^{18}O abundance that is larger than that of O$_2$ would be difficult to explain and would speak against an extended O$_2$ emission region.

The O$_2$ 119 GHz Odin line shares the LSR-velocity with that of intensity maxima in C^{18}O and N$_2$H$^+$ (this paper and Di Francesco et al. 2004, 2009). It seems therefore reasonable to identify the location of predominant O$_2$ emission with the central parts of the cold core ρ Oph A, i.e. the region including P 2 and P 3 (SM 1N and SM 1, respectively) with a probable extent on the 30″ to 1′ scale.

5. Conclusions

Summarising, we briefly conclude the following:

- C^{18}O (3−2) mapping observations with APEX of a 10′ × 5′ region in ρ Oph A have revealed a complex radial velocity field. The central 200″ × 200″ have been spatially sampled at the Nyquist frequency.
- The υ_{LSR} of the O$_2$ 119 GHz line appears confined to a particular region (SM 1), which is also a prime emitter in C^{18}O and N$_2$H$^+$.
- The observation of O^{18}O toward SM 1 (P 3) and SM 1N (P 2) resulted in upper limits. Combined with the C^{18}O data and for temperatures below 30 K, this leads to a ratio of N(C^{18}O)/N(O^{18}O) > 16 .
- From the O$_2$ and O^{18}O observations we infer an O$_2$ abundance $5 \times 10^{-7} < X$(O$_2$) $\lesssim 2.5 \times 10^{-6}$.

- The O$_2$ source is likely relatively compact, on the arcminute or smaller scale, and should become readily detectable by upcoming Herschel HIFI observations.

References

André, Ph., Ward-Thompson, D, & Barsony M. 1993, ApJ, 406, 122
Asplund, M., Grevesse, N., Sauval, A. J., & Scott P. 2009, ARA&A, 47, 481
Bergin, E. A., Melnick, G. J., Stauffer, J. R., et al. 2000, ApJ, 539, L 129
Bergman, P. 1995, ApJ, 445, L 167
Bensch, F., Pak I., Wouterloot, J. G. A., Klapper, G., & Winnewisser, G. 2001, ApJ, 562, L 185
Black, J. H., & Smith, P. L. 1984, ApJ, 277, 562
Carty, D., Goddard, A., Köhler, S. P. K., et al. 2006, JPhChA, 110, 3101
Charnley, S. B., Rodgers, S. D., & Ehrenfreund, P. 2001, A&A, 378, 1024
Di Francesco, J., André, P., & Myers, P. C. 2004, ApJ, 617, 425
Di Francesco, J., André, P., & Myers, P. C. 2009, ApJ, 700, 1994
Federman, S. R., Lambert, D. L., Sheffer, Y., et al. 2003, ApJ, 591, 986
Fuchs, G. W., Cuppen, H. M., Ioppolo, S., et al. 2009, A&A, 505, 629
Fuente, A., Cernicharo, J., Garcia-Burillo, S., & Tejero, J. 1993, A&A, 275, 558
Goldsmith, P. F., & Langer, W. D. 1978, ApJ, 222, 881
Goldsmith, P. F., Snell, R. L., Erickson, N. R., et al. 1985, ApJ, 289, 613
Goldsmith, P. F., Melnick, G. J., Bergin, E. A., et al. 2000, ApJ, 539, L 123
Hollenbach, D., Kaufman, M. J., Bergin, E. A., & Melnick, G. J. 2009, ApJ, 690, 1497
Ioppolo, S., Cuppen, H. M., Romanzin, C., van Dishoeck, E. F., & Linnartz, H. 2008, ApJ, 686, 1474
Johnstone, D., Wilson, C. D., Moriarty-Schieven, G., et al. 2000, ApJ, 545, 327
Klapper, G., Surin, L., Lewen, F., et al. 2003, ApJ, 582, 262
Larsson, B., Liseau, R., Pagani, L., et al. 2007, A&A, 466, 999
Liseau, R., & Justtanont, K. 2009, A&A, 499, 799
Liseau, R., Lorenzetti, D., Molinari, S., et al. 1995, A&A, 300, 493
Liseau, R., White, G. J., Larsson, B., et al. 1999, A&A, 344, 342
Liseau, R., Larsson, B., Brandeker, A., et al. 2003, A&A, 402, L 73
Liseau, R., et al. 2005, in Recent Successes and Current Challenges, ed. D. C. Lis, G. A. Blake, & E. Herbst, IAU Symp., 231, 301
Liszt, H. S., & Vanden Bout, P. A. 1985, ApJ, 291, 178
Loren, R.B., Wootten, A., & Wilking, B. A. 1990, ApJ, 365, 269
Maréchal, P., Viala, Y. P., & Benayoun, J. J. 1997a, A&A, 324, 221
Maréchal, P., Viala, Y. P., & Pagani, L. 1997b, A&A, 328, 617
Maruta, H., Nakamura, F., Nishi, R., Ikeda, N., & Kitamura, Y. 2009, [arXiv:0907.2558]
Matar, E., Congiu, E., Dulieu, F., Momeni, A., & Lemaire, J. L. 2008, A&A, 492, L 17
Motte, F., André, P., & Neri, R. 1998, A&A, 336, 150
Pagani, L., Olofsson, A. O. H., Bergman, P., et al. 2003, A&A, 402, L 77
Pankonin, V., & Walmsley, C. M. 1978, A&A, 64, 333
Quan, D., Herbst, E., Millar, T. J., et al. 2008, ApJ, 681, 1318
Quéméner, G., Balakrishnan, N., & Kendrick, B. K. 2009, PhRvA, 79, 022703
Risacher, C., Vassilev, V., Monje, R., et al. 2006, A&A, 454, L 17
Roberts, H., & Herbst, E. 2002, A&A, 395, 233
Schinke, R., Engel, V., Buck, U., Meyer, H., & Diercksen, G. H. F. 1985, ApJ, 299, 939
Spaans, M., & van Dishoeck, E. F. 2001, ApJ, 548, L 217
Steinbach, W., & Gordy, W. 1975, PhRvA, 11, 729
Vassilev, V., Meledin, D., Lapkin, I., et al. 2008, A&A, 490, 1157
Viti, S., Roueff, E., Hartquist, T. W., Pineau des Forêts G., & Williams D. A. 2001, A&A, 370, 557
Wannier, P. G. 1980, ARA&A, 18, 399
Willacy, K., Langer, W. D., & Allen, M. 2002, ApJ, 573, L 119
Xu, C., Xie, D., Honvault, P., Lin, S. Y., & Guo, H. 2007, JChPh, 127, 024304

---

[8] This C^{18}O column density, which represents an average over ten arcminutes, implies an H$_2$ column density, N(H$_2$) $\sim 2.5 \times 10^{22}$ cm^{-2}, a value which has been derived also by other means (Larsson et al. 2007, and references therein). At the adopted distance of 120 pc, this translates into an H$_2$-mass of the ρ Oph A cloud of $\gtrsim 30 M_\odot$. Not totally unexpected, most of the mass would be contributed on larger scales (cf., e.g., Motte et al. 1998; Maruta et al. 2009).